2024 IEEE International Conference on Robotics and Automation (ICRA 2024)
May 13-17, 2024. Yokohama, Japan

A Backdrivable Axisymmetric Kinematically Redundant (6+3)-Degree-of-Freedom Hybrid Parallel Manipulator

Jehyeok Kim and Clément Gosselin, *Fellow, IEEE*

***Abstract*— A kinematically redundant (6+3)-degree-of-freedom (DOF) hybrid parallel robot with an axisymmetric workspace is proposed. By arranging the first revolute joint of each leg such that they have the same rotation axis, this robot can achieve an axisymmetric workspace, resulting in a large reachable workspace. In addition, type II singularities, which critically limit the orientational workspace, can be fully avoided by utilizing kinematic redundancy. A gripper mechanism is developed to increase the orientational workspace by exploiting the redundant DOFs. Moreover, the orientational workspace can be further increased by controlling one of the redundant DOFs to keep a certain constant angle. As a result, the proposed hybrid parallel robot achieves a high workspace-to-footprint ratio comparable to that of serial robots. A CAD model of the robot and computer animations are provided to demonstrate the large workspaces and the gripper mechanism. A significant advantage of the proposed robot over serial architectures is that the robot is backdrivable since it uses direct-drive or quasi-direct-drive actuators.**

I. INTRODUCTION

Parallel robots are well known for their advantages of high speed and acceleration, improved accuracy, and high payload capacity. In addition, this type of robot is beneficial for increasing physical interaction performance owing to its low moving inertia. However, a critical drawback of parallel robots is the limited size of reachable and orientational workspaces compared to serial robots of similar scale. Since the robot's moving platform is connected to multiple legs, the workspaces of the robot are easily restricted by interference between legs and the limited intersection area of each leg. Type II singularities of parallel robots also deteriorate the orientational workspace, which the geometric scaling of robots cannot solve. Moreover, a disadvantage of parallel robots is a relatively large footprint. Indeed, the low workspace-to-footprint ratio is the main reason for reducing the usefulness of parallel robots.

As an approach to increasing the workspace-to-footprint ratio, several studies introduced parallel architectures with an axisymmetric workspace. This approach, which can be achieved by making the connection between a base and the robot to only have one rotational axis, is advantageous for securing a large reachable workspace because each leg can rotate about the same axis. In [1] and [2], the authors proposed a 3-degree-of-freedom (DOF) parallel architecture with an axisymmetric workspace by modifying the leg configuration of the delta robot. In [3], the authors suggested a 4-DOF SCARA robot with two RRR legs and an RP leg for a cylindrical workspace without a void. In [4]–[7], 5-DOF and 6-DOF parallel architectures were proposed by utilizing coaxially actuated upper arms. Although these robots achieved a large reachable workspace, type II singularities greatly limit their orientational workspace and this issue was not addressed.

Recently, kinematically redundant parallel architectures have been investigated to overcome type II singularities. Using kinematic redundancy, the legs of parallel robots can avoid configurations that cause type II singularities for an arbitrary configuration of the moving platform. In [8] and [9], [10], it was shown that planar parallel architectures with respectively 1 and 3 redundant DOFs can avoid all type II singularities. Spatial kinematic redundant architectures with the same capability were proposed in [11]–[16]. In each study, the architectures can successfully achieve a large orientational workspace owing to singularity avoidance. However, the legs of these architectures are fixed in distributed locations like traditional parallel robots, so the size of the reachable workspace is still limited.

Our research goal is to develop a parallel or hybrid parallel robot with a large reachable and orientational workspace and a small footprint, comparable to that of serial robots. To achieve this, we devised a novel kinematically redundant (6+3)-DOF hybrid parallel architecture with an axisymmetric workspace. This architecture has 3 redundant DOFs and three legs of RRRSR architecture, where R, R, and S represent an actuated revolute joint, a passive revolute joint and a spherical joint, respectively. By arranging the first revolute joints of each leg (i.e., the only joints that are fixed to the base) to have the same axis of rotation, the axisymmetric workspace and the small footprint could be achieved. As suggested in [14], this architecture also utilizes the first redundant DOF to remotely operate the open/close function of an integrated gripper.

Moreover, we propose a gripper mechanism that further exploits the second redundant DOF to expand the orientational workspace. Indeed, in addition to the rotatable angular range of the moving platform, our gripper's finger base frame can be rotated independently from the moving platform by a rotation of the second redundant DOF. Furthermore, the rotation of the redundant DOF is amplified by a gear transmission mechanism to generate more rotation of the finger base. As a result, the rotation range of the moving platform with respect to the rotation axis of the finger base can be further increased by controlling the second redundant DOF.

*The financial support of the Natural Sciences and Engineering Research Council of Canada (NSERC) is gratefully acknowledged.

The authors are with the Department of Mechanical Engineering, Université Laval, Québec, Qc, Canada, jehyeok.kim.1@ulaval.ca, gosselin@gmc.ulaval.ca

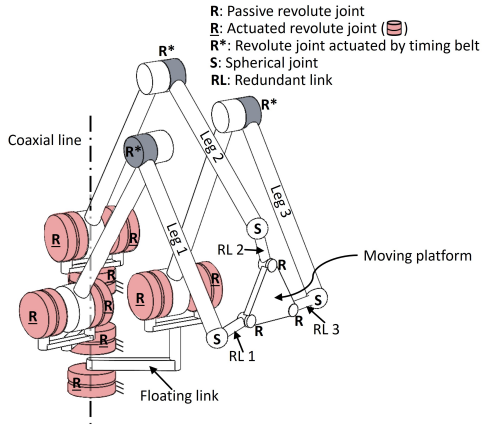

Fig. 1. Architecture of the proposed hybrid parallel robot.

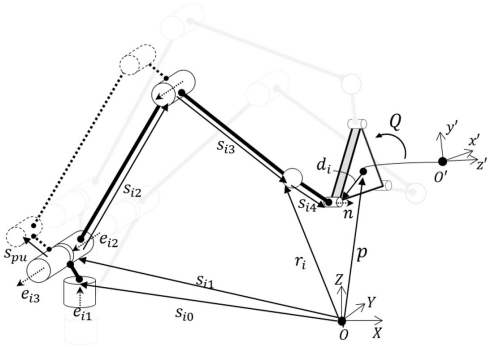

Fig. 2. Geometrical description of the proposed robot.

At last, the third redundant DOF is utilized to increase the rotation range of the other redundant DOFs. Originally, each redundant DOF had a restricted rotation range of 120 degrees for type II singularity avoidance. We found that if one redundant DOF maintains a certain angle, the rotation range of the remaining two redundant DOFs can be increased to 180 degrees. Consequently, this function of the third redundant DOF increases the amount of rotation range of the finger base generated by the gripper mechanism above. The estimated masses of the entire robot and gripper are 17 kg and 1.5 kg, respectively. Due to the actuators being fixed to the base or having a small moment arm to the base, the masses of the actuators and their mounting structures were excluded when estimating the effective moving mass, resulting in a total of 4.5 kg. The proposed robot is designed to achieve a payload of 3 kg, excluding the gripper mass, with a maximum speed of 1 m/s and a maximum acceleration of 10 m/s².

This paper is structured as follows. Section II explains the proposed robot architecture. In Section III, kinematic modelling and singularity analysis are presented. The gripper mechanism utilizing redundancy is introduced in Section IV. Section V shows the analyzed reachable and orientational workspaces of the robot. Section VI introduces the contents of CAD demonstrations of a virtual prototype. Finally, Section VII concludes this article.

II. Robot Architecture

As illustrated in Fig. 1, The architecture of the proposed robot consists of a moving platform and three kinematically identical legs. Each leg can be considered as a combination of an RRR chain and an RS chain. The RRR chain generates 3-DOF positional motion of the S joint. The RS chain, which is denoted as a redundant link, connects the RRR chain to the moving platform and generates redundancy. Fig. 2 shows a geometrical description of one leg. $\mathbf{s}_{ij}$ denotes a vector along the jth link of the ith leg, which has a length of $\mathbf{l}_{ij}$. $\mathbf{e}_{ij}$ is a unit vector along the axis of the corresponding joint.

The first R joints of each leg are fixed to the ground while their rotation axes have a coaxial line forming a central column of the actuators. The second and third R joints having the same axis of rotation are connected to the first R joint through floating links. This rotation axis of the second and third R joints is perpendicular to the axis of the first R joint. As illustrated in Fig. 1, the floating links for leg 1 and leg 3 have an angled shape to avoid interference with the central column. The second actuated joint rotates a proximal link directly. Unlike typical parallel robots using a 5-bar planar linkage architecture to rotate the distal link, the proposed robot has a timing pulley/belt mechanism to minimize interference between legs. Since the RRR chain of each leg forms a vertical work plane, the workspace deterioration due to interference between legs and work environments can be greatly reduced.

The redundant link is connected to the distal link by an S joint and to the moving platform by an R joint. The R joints of each redundant link are located on the vertices of a triangular end-effector and have parallel axes. The total number of actuated revolute joints is 9. Even though the moving platform has 6-DOFs, each redundant link generates an additional 1-DOF, so the total number of DOFs for the proposed robot is 9. Therefore, the proposed robot does not have actuation redundancy that causes antagonistic forces in the structure. Furthermore, the robot can avoid configurations that cause type II singularities by utilizing the redundant DOFs.

III. Kinematic Modelling and Singularity Analysis

A. Kinematic modelling of the proposed robot

Through kinematic modelling, we derive the Jacobian matrices which provide the relation between a vector of Cartesian velocities of the moving platform and a vector of actuated joint velocities. Since the proposed robot architecture is essentially the same as that of the robot proposed in [14] in terms of kinematic modelling, the detailed equations of this reference can be used. Nevertheless, this section briefly introduces the kinematic model of the proposed robot to clearly describe the architecture. As shown in Fig. 2, a global frame and local frame attached to the centroids of the base and moving platform are described as $OXYZ$ and $O'x'y'z'$, respectively. Vector $\mathbf{p}$ represents the position of O' with respect to O. Vector $\mathbf{r}_i$ is the position of the spherical

joint with respect to O. Vector $\mathbf{n}$ denotes the unit vector along the axis of the R joint of the redundant links. Vector $\mathbf{d}_i$ represents the position of the R joint of the ith redundant link. $\boldsymbol{Q}$ is the orientation of the moving platform with respect to the fixed frame. All vectors are expressed in the global coordinate frame, except for $\mathbf{d}_i$, which is expressed in the local frame. To derive the kinematic model, two geometrical constraint equations of each leg are formulated, resulting in six constraint equations. The first constraint equation which expresses that the length of the redundant link is constant is written as,

$$(\mathbf{p} + \boldsymbol{Q}\mathbf{d}_i - \mathbf{r}_i)^T(\mathbf{p} + \boldsymbol{Q}\mathbf{d}_i - \mathbf{r}_i) = |\mathbf{s}_{i4}|^2. \tag{1}$$

Also, the redundant link must be orthogonal to vector $\mathbf{n}$ which yields

$$\mathbf{n}^T(\mathbf{p} + \boldsymbol{Q}\mathbf{d}_i - \mathbf{r}_i) = 0. \tag{2}$$

In (1) and (2), index i refers to the legs with values 1, 2 and 3. The time derivative of (1) yields,

$$\mathbf{s}_{i4}^T\dot{\mathbf{p}} + [(\boldsymbol{Q}\mathbf{d}_i) \times \mathbf{s}_{i4}]\boldsymbol{\omega} = \mathbf{s}_{i4}^T\dot{\mathbf{r}}_i. \tag{3}$$

To express $\dot{\mathbf{r}}_i$ in the right-hand side of (3), the relation equation between a vector of Cartesian velocities of the spherical joint and a vector of actuated joint velocities is required. As shown in Fig. 2, the timing pulley/belt mechanism is represented as the virtual 5-bar linkage and the radius of the timing pulley is denoted by $\mathbf{s}_{pu}$. Using the detailed derivation in [14], the relation is written as follows,

$$\dot{\mathbf{r}}_i = \mathbf{J}_i^{-1}\mathbf{W}_i\dot{\boldsymbol{\theta}}_i, \tag{4}$$

where

$$\mathbf{J}_i = \begin{bmatrix} \mathbf{e}_{i2}^T \\ \mathbf{s}_{i3}^T \\ -\frac{l_{pu}}{l_{i3}}\mathbf{s}_{i2}^T \end{bmatrix} \tag{5}$$

and

$$\mathbf{W}_i = \begin{bmatrix} \omega_{i11} & 0 & 0 \\ 0 & \mathbf{s}_{i3}^T(\mathbf{e}_{i2} \times \mathbf{s}_{i2}) & 0 \\ 0 & \omega_{i32} & \mathbf{s}_{i2}^T(\mathbf{e}_{i3} \times \mathbf{s}_{pu}) \end{bmatrix} \tag{6}$$

with

$$\omega_{i11} = (\dot{\mathbf{r}}_\mathbf{i} - \mathbf{s}_{\mathbf{i1}})^T(\mathbf{e}_{i2} \times \mathbf{e}_{i1}) \tag{7}$$

$$\omega_{i32} = (1 + \frac{l_{pu}}{l_{i3}})\mathbf{s}_{\mathbf{i5}}{}^T(\mathbf{s}_{i2} \times \mathbf{e}_{i2}). \tag{8}$$

By substituting (4) into (3), the kinematics of the global robot is derived as,

$$\begin{bmatrix} \mathbf{s}_{14}^T & [(\boldsymbol{Q}\mathbf{d}_1) \times \mathbf{s}_{14}]^T \\ \mathbf{s}_{24}^T & [(\boldsymbol{Q}\mathbf{d}_2) \times \mathbf{s}_{24}]^T \\ \mathbf{s}_{34}^T & [(\boldsymbol{Q}\mathbf{d}_3) \times \mathbf{s}_{34}]^T \end{bmatrix} \begin{bmatrix} \dot{\mathbf{p}} \\ \boldsymbol{\omega} \end{bmatrix} = \begin{bmatrix} \mathbf{k}_1^T & \mathbf{0}^T & \mathbf{0}^T \\ \mathbf{0}^T & \mathbf{k}_2^T & \mathbf{0}^T \\ \mathbf{0}^T & \mathbf{0}^T & \mathbf{k}_3^T \end{bmatrix} \begin{bmatrix} \dot{\boldsymbol{\theta}}_1 \\ \dot{\boldsymbol{\theta}}_2 \\ \dot{\boldsymbol{\theta}}_3 \end{bmatrix} \tag{9}$$

where

$$\mathbf{k}_i^T = \mathbf{s}_{i4}^T\mathbf{J}_i^{-1}\mathbf{W}_i, i = 1, 2, 3. \tag{10}$$

and $\mathbf{0}^T$ represents a zero vector of dimension 1×3. $\dot{\boldsymbol{\theta}}_i = [\dot{\theta}_{i1}\dot{\theta}_{i2}\dot{\theta}_{i3}]^T$ is a vector of three actuated joint velocities of ith leg with dimension of 3×1.

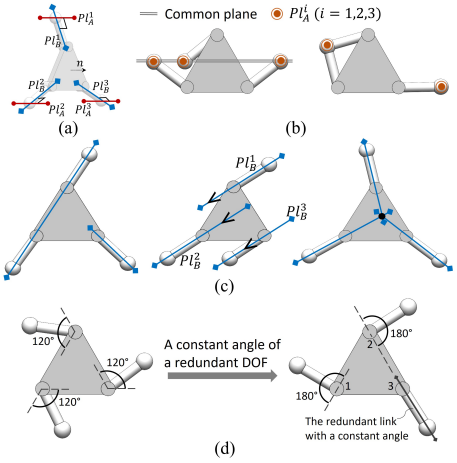

Fig. 3. Type II Singularity analysis. (a) Description of the Plücker lines. (b) Singular conditions of matrix $\mathbf{J}_A$. The common plane is perpendicular to the moving platform. (c) Singular conditions of matrix $\mathbf{J}_B$. (d) The effect of a redundant DOF with a certain constant angle.

Next, the time derivative of (2) is written as

$$\mathbf{n}^T\dot{\mathbf{p}} + (\mathbf{c}_i \times \mathbf{n})^T\boldsymbol{\omega} = \mathbf{n}^T\dot{\mathbf{r}}_i, \tag{11}$$

where

$$\mathbf{c}_i = \boldsymbol{Q}\mathbf{d}_i - \mathbf{s}_{i4}. \tag{12}$$

Using (4), the right-hand side of (11) is expressed as

$$\mathbf{k}_{i+3}^T = \mathbf{n}^T\mathbf{J}_i^{-1}\mathbf{W}_i.i = 1, 2, 3. \tag{13}$$

By substituting (13) into (11), the three velocity equations obtained from the second constraint equation are as follows,

$$\begin{bmatrix} \mathbf{n}^T & (\mathbf{c}_1 \times \mathbf{n})^T \\ \mathbf{n}^T & (\mathbf{c}_2 \times \mathbf{n})^T \\ \mathbf{n}^T & (\mathbf{c}_3 \times \mathbf{n})^T \end{bmatrix} \begin{bmatrix} \dot{\mathbf{p}} \\ \boldsymbol{\omega} \end{bmatrix} = \begin{bmatrix} \mathbf{k}_4^T & \mathbf{0}^T & \mathbf{0}^T \\ \mathbf{0}^T & \mathbf{k}_5^T & \mathbf{0}^T \\ \mathbf{0}^T & \mathbf{0}^T & \mathbf{k}_6^T \end{bmatrix} \begin{bmatrix} \dot{\boldsymbol{\theta}}_1 \\ \dot{\boldsymbol{\theta}}_2 \\ \dot{\boldsymbol{\theta}}_3 \end{bmatrix}. \tag{14}$$

Finally, the Jacobian matrices are derived by combining (9) and (14) as

$$\mathbf{J}\mathbf{t} = \mathbf{K}\dot{\boldsymbol{\theta}} \tag{15}$$

where $\mathbf{t}$ denotes $[\dot{\mathbf{p}}^T\boldsymbol{\omega}^T]^T$, $\dot{\boldsymbol{\theta}}$ is $[\dot{\boldsymbol{\theta}}_1\dot{\boldsymbol{\theta}}_2\dot{\boldsymbol{\theta}}_3]^T$ and matrices $\mathbf{J}$ and $\mathbf{K}$ are written as

$$\mathbf{J} = \begin{bmatrix} \mathbf{s}_{14}^T & [(\boldsymbol{Q}\mathbf{d}_1) \times \mathbf{s}_{14}]^T \\ \mathbf{n}^T & (\mathbf{c}_1 \times \mathbf{n})^T \\ \mathbf{s}_{24}^T & [(\boldsymbol{Q}\mathbf{d}_2) \times \mathbf{s}_{24}]^T \\ \mathbf{n}^T & (\mathbf{c}_2 \times \mathbf{n})^T \\ \mathbf{s}_{34}^T & [(\boldsymbol{Q}\mathbf{d}_3) \times \mathbf{s}_{34}]^T \\ \mathbf{n}^T & (\mathbf{c}_3 \times \mathbf{n})^T \end{bmatrix} \tag{16}$$

$$\mathbf{K} = \begin{bmatrix} \mathbf{k}_1^T & \mathbf{0}^T & \mathbf{0}^T \\ \mathbf{k}_4^T & \mathbf{0}^T & \mathbf{0}^T \\ \mathbf{0}^T & \mathbf{k}_2^T & \mathbf{0}^T \\ \mathbf{0}^T & \mathbf{k}_5^T & \mathbf{0}^T \\ \mathbf{0}^T & \mathbf{0}^T & \mathbf{k}_3^T \\ \mathbf{0}^T & \mathbf{0}^T & \mathbf{k}_6^T \end{bmatrix}. \tag{17}$$

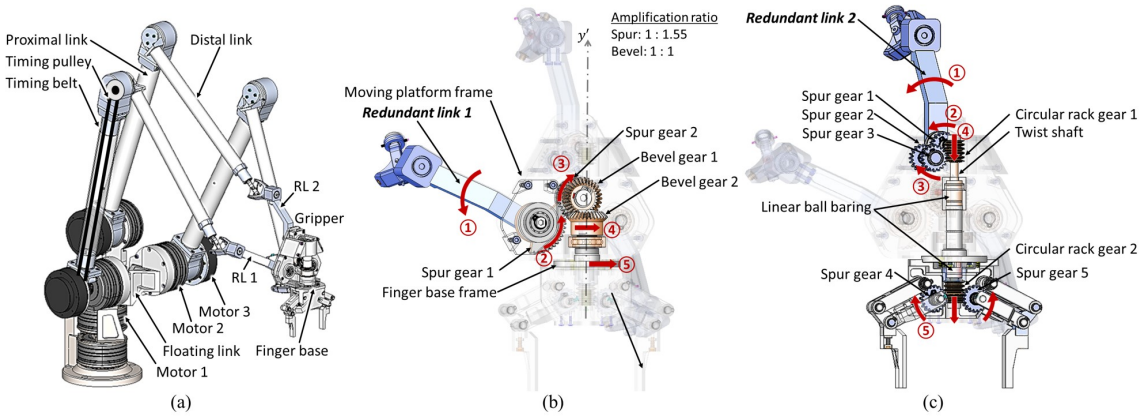

Fig. 4. (a) Implementation design of the proposed robot. The redundant link 3 (RL 3) is hidden behind the gripper. The RL 3 is connected to the gripper frame via a simple revolute joint. (b) Additional rotating function generated by redundant link 1. (c) Finger open/close function generated by redundant link 2.

B. Singularity Analysis

The type I and II singularities of a leg occur when $\mathbf{W}_i$ of (9) and $\mathbf{J}_i$ of (5) are singular, respectively. In practice, these singularities can be avoided by a proper dimensioning of linkages. The configurations causing these singularities and their avoidance were addressed in detail in [14]. The type II singularities of the moving platform that can occur in the robot configurations correspond to singular conditions of matrix $\mathbf{J}$ of (16). To simplify the singularity analysis, matrix $\mathbf{J}$ is expressed in the local coordinates of the moving platform and divided into two matrices as

$$\mathbf{J}_A = \begin{bmatrix} 0 & 0 & 1 & a_1 & b_1 & 0 \\ 0 & 0 & 1 & a_2 & b_2 & 0 \\ 0 & 0 & 1 & a_3 & b_3 & 0 \end{bmatrix} \tag{18}$$

and

$$\mathbf{J}_B = \begin{bmatrix} f_4 & g_4 & 0 & 0 & 0 & h_4 \\ f_5 & g_5 & 0 & 0 & 0 & h_5 \\ f_6 & g_6 & 0 & 0 & 0 & h_6 \end{bmatrix}. \tag{19}$$

The sub-matrices $\mathbf{J}_A$ and $\mathbf{J}_B$ consist of rows 2, 4 and 6 and rows 1,3 and 5 of matrix $\mathbf{J}$, respectively. Since these two matrices are completely independent from each other, the singular conditions of $\mathbf{J}$ can be identified separately as the conditions for which either $\mathbf{J}_A$ or $\mathbf{J}_B$ loses rank. Each row of the sub-matrices can be expressed as a geometrical line of Plücker coordinates. The Plücker lines of matrix $\mathbf{J}_A$ are parallel to $\mathbf{n}$ and pass through the centre of the spherical joints. The Plücker lines of matrix $\mathbf{J}_B$ have the same directions as their corresponding redundant link. In Fig. 3(a), the Plücker lines are illustrated as Pl^i_A and Pl^i_B where i denotes each row of the sub-matrices. According to Grassmann line geometry (GLG), the sub-matrices lose their rank when 1) the three lines are parallel to each other in the common plane, 2) the three lines, which are in common plane, have a common intersection point, 3) any two lines among three lines coincide. Fig. 3(b) and (c) show the configurations of the redundant links corresponding to the singular conditions. It was proved that all of the type II singular conditions can be avoided by restricting the redundant DOF in a 120-degree rotation range [14], as illustrated in the left side image of Fig. 3(d).

Here, we propose a method to extend the rotation range of the redundant DOF. Because the rotation range determines the possible configuration of each leg for singularity avoidance, an extension of this range is important to reduce the interferences between legs and increase the dynamic performance of the robot. Moreover, since we utilize the redundant DOF to generate further rotation of a gripper, the extension of the rotation range can increase this rotation range of a gripper. As illustrated in the right image of Fig. 3(d), when one redundant DOF maintains an angle that makes its redundant link point to the R joint of another redundant DOF, the rotation ranges of the two free redundant DOFs are increased to 180 degrees. For example, if the redundant DOF 3 points to the R joint of the redundant link 2, the intersection point always occurs at the R joint position of the redundant link 2. Therefore, if the redundant link 1 is limited to a rotation range that does not pass the straight line connecting R joints 1 and 2, the three Pl^i_B lines cannot meet at a common intersection point. At the same time, if the redundant link 2 is limited to a rotation range that does not pass the straight line connecting R joints 2 and 3, the three Pl^i_B lines cannot be parallel to each other. Consequently, when one redundant DOF maintains the aforementioned angle, the rotation angles of the two remaining redundant DOFs increase to 180 degrees.

IV. Gripper Mechanism

The redundant DOFs that overcome the type II singularities to ensure a large orientational workspace can be further exploited to generate additional functions of a gripper. As shown in the singularity analysis, except for the redundant DOF with a constant angle, the remaining two redundant DOFs can rotate freely within a range of 180 degrees. Therefore, the two redundant DOFs can be considered as remotely

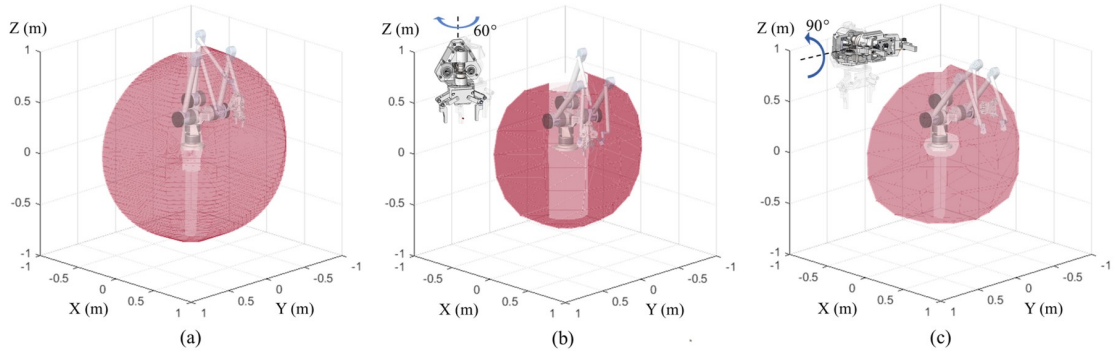

Fig. 5. Workspace analysis of the proposed robot. (a) Reachable workspace. (b) Constant orientation workspace when the moving platform rotates 60 degrees around the Z axis. (c) Constant orientation workspace when the moving platform rotates 90 degrees around the Y axis.

controlled actuators. Moving on from our previous studies that achieved only one function of the gripper, the proposed gripper mechanism is developed to have three functions by fully utilizing the redundancy. The first function is finger open/close generation. The second function is a generation of finger base rotation which is called a finger base twist. The last function is the expansion of the rotation ranges of the other redundant DOFs by maintaining a constant angle.

The implementation design of the proposed robot is illustrated in Fig. 4(a). Three actuators of each leg control the position of each spherical joint. Motor 2 actuates the proximal link of a leg. The distal link is driven by motor 3 through a timing belt which is installed inside of the proximal link. The angles of each redundant DOF are determined by the position control of each spherical joint. The twist generation and finger open/close functions are assigned to the redundant links 1 and 2, respectively. The redundant link 3 performs the third function.

The twist rotation by the redundant link 1 is generated in the following sequences (see Fig. 4(b)). Since the finger base where finger links are installed is separated from the gripper base, it can rotate independently. The axis of the twist is y' of the local frame. When redundant link 2 rotates clockwise, spur gear 1 connected to the link rotates. The rotation of spur gear 1 is transmitted to spur gear 2, resulting in the rotation of bevel gear 1. Because the finger base is connected to the bevel gear 2, the rotation of the bevel gear 1 rotates the bevel gear 2 resulting in the rotation of the finger base. The rotation of this finger base can further expand the orientation workspace determined by the configuration of the moving platform in the twist direction. There is an amplification ratio of 1.5 between spur gears 1 and 2 so that the rotation range of the redundant 180 degrees produces 270 twist rotations.

Next, the finger open/close function is achieved in the following order (see Fig. 4(c)). When redundant link 2 rotates clockwise, connected spur gear 1 rotates about the axis of the corresponding redundant DOF. The rotation of spur gear 1 makes the rotation of spur gear 3 through spur gear 2. The rotational motion of the spur gear 3 creates an upward linear motion of the shaft connected with the circular rack gear. The linear motion of the circular rack gear connected on the opposite side of this axis generates a rotational motion of spur gear 4, resulting in fingers opening. By the same process, counterclockwise rotation of the redundant link closes the finger. During this transmission process, the amount of rotation is maintained and the finger rotates as much as the redundant link rotates. Since the two functions are mechanically separated, each function can be controlled independently. This gripper design is advantageous for reducing its mass and the complexity of electrical or pneumatic wiring because it utilizes the moving platform of the parallel robot as the main frame and the kinematic redundancy to create functionality without additional actuators.

V. Workspace Analysis

The evaluation of the workspace consists of reachable workspace, constant orientation workspace and orientational workspace analysis. The links and joints are considered as straight-line segments and points, respectively in a simulation model to reduce a computational burden. In addition, the angles of each redundant joint are fixed to the specific constant values for forming an equilateral triangle of the spherical joints. Since the proposed robot has an axisymmetric workspace, the evaluations are conducted only on a representative XZ plane ($X \geq 0, Y = 0$) and the results on this plane are expanded by rotating it around Z. Using polar coordinates, the simulation intervals of radius and rotation angle to Y axis are set to 1mm, 3 degrees for the outer boundary area and 5 mm, 18 degrees for the inner boundary area. The mechanical interferences between the proximal, distal and redundant links are considered in this analysis.

Fig. 5(a) shows the axisymmetric reachable workspace of the robot. The reachable workspace means all positions that can be reached by the moving platform with at least one orientation. Due to the interference between the column structure and the floating frame, the angle range of the axial symmetry is limited to about $\pm$ 110 degrees. Inside the reachable workspace, there is a cylindrical hole because of type I singularities that occur when the spherical joint of the central leg is located on the axis of rotation of the first actuator. The constant orientation workspaces of the robot are illustrated in Fig. 5(b) and (c). A constant orientation workspace refers to all positions that can be reached by

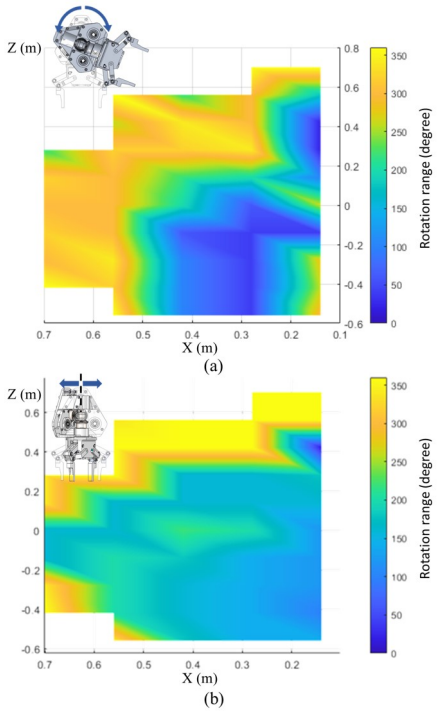

Fig. 6. (a) Orientational workspace with respect to the X axis rotation. (b) Orientational workspace with respect to the Z axis rotation.

the moving platform when the orientation of the platform is kept constant. Fig. 5(b) represents the constant orientation workspace when the moving platform is rotated 60 degrees around the global Z axis from its reference orientation. This constant orientation workspace has a reduced volume compared to the reachable workspace. In particular, there is a large cylindrical hole at the centre of the workspace due to the interference. Fig. 5(c) illustrates the constant orientation workspace when the moving platform is rotated 90 degrees around the global Y axis. Although the volume of the workspace is smaller, the shape feature of the central cylindrical hole is similar to that of the reachable workspace.

Next, the orientational workspace is analyzed. Because type II singularities can be completely avoided through kinematic redundancy, we focus on the interferences between links restricting the workspace. Fig. 6(a) and (b) show the orientational workspaces with respect to the global X and Z rotations of the moving platform, respectively. The colour of the graph indicates the rotational range of the moving platform. The average rotational range of X axis rotation is 198 degrees. As shown in Fig. 6(a), the X axis rotation range shows significant differences depending on the location within the workspace. Near the outer boundary, a wide rotation of about 300 degrees is possible, while only a narrow rotation of about 50 degrees is possible at the bottom right and top right. Through a visual representation of the robot configuration at each location, the reasons for the narrow rotation range are identified. For the bottom right area, the interference between the distal link of the central leg and the proximal links of the side legs is a restricting factor. The interference between the proximal link of the central leg and the proximal links of the side legs mainly limits the rotational range at the top right area. The average rotational range of Z axis rotation is 192 degrees. Although this value is lower than that of the Z axis rotation case, the rotational ranges are distributed more uniformly in the workspace. Especially, since the gripper mechanism can generate an additional 270 degrees of rotation around the Z axis, one revolution of the gripper can be achieved at almost all positions, resulting in enough reorientation range of a gripped object.

VI. Video Animations of the Virtual Prototype

The animation of the CAD model of the prototype is provided as supplemental material to explain the robot and gripper motions in more detail. At first, the animation demonstrates translational motions in the XZ plane. Second, the rotational motion of the robot around the X-axis is demonstrated to show the axisymmetric workspace. Next, the orientational motions of the moving platform are presented. The last part presents finger open/close and twist functions which are remotely controlled by the actuators mounted near the base.

VII. Conclusion

In this article, we propose an axisymmetric kinematically redundant (6+3)-DOF hybrid parallel robot for increasing the ratio of workspace to footprint while allowing mechanical backdrivability. The axisymmetric workspace is achieved by placing the first actuator of each leg coaxially. By the kinematic redundancy, the proposed robot can fully avoid type II singularities resulting in a large orientational workspace. Moreover, we suggest a method of utilizing a redundant DOF to further expand the orientation workspace. When one of the redundant DOFs is fixed to a certain angle, the rotation ranges of the remaining redundant DOFs increase from 120 degrees to 180 degrees. In addition, the proposed gripper mechanism can generate 270 degrees of the additional rotation of the gripper around the y' axis of the moving platform. The results of workspace analysis show that the proposed robot achieves a large axisymmetric workspace. The orientational workspace analysis shows that the average rotation ranges of the moving platform about the global Y and Z axes are 198 and 192 degrees, respectively. In particular, the global Z axis rotation allows one revolution within the workspace owing to the additional rotation function of the gripper. As a result, the proposed robot achieves low moving inertia and improved accuracy, which are the advantages of parallel robots and a large translational and orientational workspace compared to the footprint. The implementation design of the prototype utilizes a quasi-direct-drive motor to ensure backdrivability. Due to these advantages, the proposed robot is ideal for physical interaction. Our future works include evaluating the physical interactive performances by measuring the bandwidth and perceived inertia of the manufactured prototype. Quantitative comparisons with conventional serial robots will be conducted using experimental results of the manufactured prototype.

REFERENCES

[1] K. Marlow, M. Isaksson, H. Abdi, and S. Nahavandi, "Workspace analysis of two similar 3-dof axis-symmetric parallel manipulators," in *2014 IEEE/RSJ International Conference on Intelligent Robots and Systems*, 2014, pp. 1690–1696.

[2] M. Isaksson, "A family of planar parallel manipulators," in *2011 IEEE international conference on robotics and automation*. IEEE, 2011, pp. 2737–2744.

[3] O. Stepanenko and I. A. Bonev, "Novel 4-dof scara parallel robot with cylindrical workspace," in *International Design Engineering Technical Conferences and Computers and Information in Engineering Conference*, vol. 51807. American Society of Mechanical Engineers, 2018, p. V05AT07A047.

[4] M. Isaksson and M. Watson, "Workspace Analysis of a Novel Six-Degrees-of-Freedom Parallel Manipulator With Coaxial Actuated Arms," *Journal of Mechanical Design*, vol. 135, no. 10, p. 104501, 07 2013. [Online]. Available: https://doi.org/10.1115/1.4024723

[5] M. Isaksson, T. Brogårdh, I. Lundberg, and S. Nahavandi, "Improving the kinematic performance of the scara-tau pkm," in *2010 IEEE International Conference on Robotics and Automation*. IEEE, 2010, pp. 4683–4690.

[6] T. Brogårdh, S. Hanssen, and G. Hovland, "Application-oriented development of parallel kinematic manipulators with large workspace," in *Proc. of the 2nd International Colloquium of the Collaborative Research Center 562: Robotic Systems for Handling and Assembly*, 2005, pp. 153–170.

[7] S. Sakurai and S. Katsura, "A new design of redundant 7-dof parallel robot with large workspace," in *2023 IEEE International Conference on Mechatronics (ICM)*, 2023, pp. 1–6.

[8] C. Gosselin, T. Laliberté, and A. Veillette, "Singularity-free kinematically redundant planar parallel mechanisms with unlimited rotational capability," *IEEE Transactions on Robotics*, vol. 31, no. 2, pp. 457–467, 2015.

[9] I. Ebrahimi, J. A. Carretero, and R. Boudreau, "3-prrr redundant planar parallel manipulator: Inverse displacement, workspace and singularity analyses," *Mechanism and Machine Theory*, vol. 42, no. 8, pp. 1007–1016, 2007.

[10] ——, "A family of kinematically redundant planar parallel manipulators," 2008.

[11] C. Gosselin and L.-T. Schreiber, "Kinematically redundant spatial parallel mechanisms for singularity avoidance and large orientational workspace," *IEEE Transactions on Robotics*, vol. 32, no. 2, pp. 286–300, 2016.

[12] J. Lacombe and C. Gosselin, "Singularity analysis of a kinematically redundant (6+ 2)-dof parallel mechanism for general configurations," *Mechanism and Machine Theory*, vol. 176, p. 105015, 2022.

[13] K. Wen, D. Harton, T. Laliberté, and C. Gosselin, "Kinematically redundant (6+ 3)-dof hybrid parallel robot with large orientational workspace and remotely operated gripper," in *2019 International Conference on Robotics and Automation (ICRA)*. IEEE, 2019, pp. 1672–1678.

[14] K. Wen, T. S. Nguyen, D. Harton, T. Laliberté, and C. Gosselin, "A backdrivable kinematically redundant (6+ 3)-degree-of-freedom hybrid parallel robot for intuitive sensorless physical human–robot interaction," *IEEE Transactions on Robotics*, vol. 37, no. 4, pp. 1222–1238, 2020.

[15] A. Yiğit, D. Breton, Z. Zhou, T. Laliberté, and C. Gosselin, "Kinematic analysis and design of a novel (6+3)-dof parallel robot with fixed actuators," in *2023 IEEE International Conference on Robotics and Automation (ICRA)*, 2023, pp. 9693–9699.

[16] J. Kim and C. Gosselin, "A kinematically redundant (6+1)-dof hybrid parallel robot for delicate physical environment and robot interaction (peri)," in *2023 IEEE International Conference on Robotics and Automation (ICRA)*, 2023, pp. 9679–9685.